









RESEARCH ARTICLE | NOVEMBER 15 2023

Evidence for intrinsic magnetic scatterers in the topological semimetal $(\text{Bi}_2)_5(\text{Bi}_2\text{Se}_3)_7$

Pascal Gehring ; Clement Merckling ; Ruishen Meng ; Valentin Fonck ; Bart Raes ; Michel Houssa ; Joris Van de Vondel ; Stefan De Gendt 



APL Mater. 11, 111116 (2023)

<https://doi.org/10.1063/5.0167544>

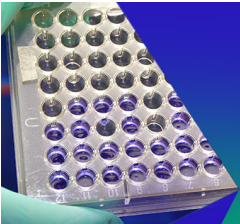


View
Online





Export
Citation

CrossMark



Biomicrofluidics
Special Topic:
Microfluidics and Nanofluidics in **India**
Submit Today



Evidence for intrinsic magnetic scatterers in the topological semimetal $(\text{Bi}_2)_5(\text{Bi}_2\text{Se}_3)_7$

Cite as: APL Mater. 11, 111116 (2023); doi: 10.1063/5.0167544

Submitted: 13 July 2023 • Accepted: 19 October 2023 •

Published Online: 15 November 2023



View Online



Export Citation



CrossMark

Pascal Gehring,^{1,2,a)} Clement Merckling,^{1,3} Ruishen Meng,⁴ Valentin Fonck,² Bart Raes,⁵
Michel Houssa,^{1,4} Joris Van de Vondel,⁵ and Stefan De Gendt^{1,6}

AFFILIATIONS

¹IMEC, Kapeldreef 75, 3001 Leuven, Belgium

²IMCN/NAPS, Université Catholique de Louvain (UCLouvain), 1348 Louvain-la-Neuve, Belgium

³KU Leuven, Departement of Material Engineering, Kasteelpark Arenberg 44, 3001 Leuven, Belgium

⁴Semiconductor Physics Laboratory, Department of Physics and Astronomy, KU Leuven, Celestijnenlaan 200D, B-3001 Leuven, Belgium

⁵Quantum Solid-State Physics, Department of Physics and Astronomy, KU Leuven, Celestijnenlaan 200D, B-3001 Leuven, Belgium

⁶KU Leuven, Department of Chemistry, Celestijnenlaan 200f, 3001 Leuven, Belgium

^{a)} Author to whom correspondence should be addressed: pascal.gehring@uclouvain.be

ABSTRACT

We report the synthesis and characterization of high-quality thin films of the topological semimetal $(\text{Bi}_2)_5(\text{Bi}_2\text{Se}_3)_7$. Cryogenic magnetotransport experiments reveal strong metallic character and spin-orbit coupling in the films. By studying the temperature dependence of the electrical resistance of the topological semimetal, we observe a pronounced Kondo effect, which points toward the presence of magnetic scatterers. With the aid of density functional theory calculations, we identify Bi vacancies as intrinsic magnetic scatterers in this topological semimetal.

© 2023 Author(s). All article content, except where otherwise noted, is licensed under a Creative Commons Attribution (CC BY) license (<http://creativecommons.org/licenses/by/4.0/>). <https://doi.org/10.1063/5.0167544>

INTRODUCTION

Topological materials are exotic quantum materials with a non-trivial band topology. They could be promising building blocks for future thin-film electronic devices with potential applications ranging from energy efficient spin-orbit torque memories,¹ to energy harvesting devices,^{2,3} to neuromorphic computing devices,⁴ or to a new generation of amplifier devices.⁵ Recently, a new model system to study topological break-down and interlayer interactions has been discovered, $(\text{Bi}_2)_n(\text{Bi}_2\text{Se}_3)_m$, a natural hetero-structure of the model 3D topological insulator Bi_2Se_3 and the 2D topological insulator Bi_2 . In bulk, it is a semimetal with Dirac-cone-like topological surface states that depend on its termination.^{6,7} Furthermore, the compound could be very valuable for future functional electronics since it possesses topological surface states even in the bi-layer limit, enabling the fabrication of ultra-thin topological devices,⁸ and it could be promising for energy harvesting applications thanks to its low thermal conductivity.⁹ Here, we experimentally reveal the presence of

magnetic scatterers in thin films of $(\text{Bi}_2)_5(\text{Bi}_2\text{Se}_3)_7$ by performing low-temperature magnetotransport experiments combined with in-depth physical analysis. Supporting first-principle simulations allow us to identify Bi vacancies as magnetic scatterers in this topological semimetal.

High-quality $(\text{Bi}_2)_5(\text{Bi}_2\text{Se}_3)_7$ thin films were grown using a plasma-assisted molecular beam epitaxy (PA-MBE) technique on $\alpha\text{-Al}_2\text{O}_3(0001)$ c axis sapphire substrates (see the supplementary material). This hybrid approach has already been successfully used for the synthesis of transition metal dichalcogenide monolayers.^{10,11} The exact composition of this hetero-structure has been determined by Rutherford backscattering spectrometry, Raman microscopy, and high-resolution transmission electron microscopy (see the supplementary material). After growth and in order to prevent surface degradation,¹² a thin (2 nm) capping layer of Al_2O_3 or CaF_2 was deposited *in situ*. No influence of the type of the capping layer on the electronic properties of the thin films was found.

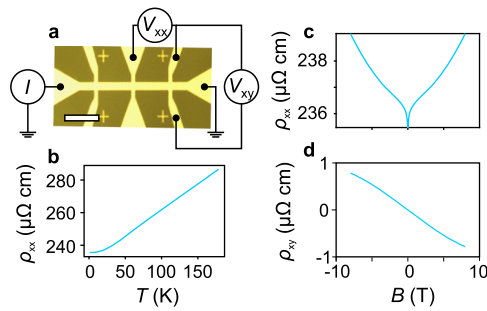


FIG. 1. (a) Optical micrograph of a typical device. A current I is applied between the source and drain lead and the resulting voltages V_{xx} and V_{xy} are measured. Scale bar: 40 μm . (b) Temperature dependent longitudinal resistivity ρ_{xx} . (c) Longitudinal and (d) transverse resistivity as a function of magnetic field measured at $T = 2$ K.

The as-grown films were patterned into Hall bar shape using standard optical lithography and dry etching/ion milling. An optical micrograph of a typical Hall bar device with dimensions $L = 100 \mu\text{m}$ and $W = 10 \mu\text{m}$ is shown in Fig. 1(a). The temperature and magnetic field dependent longitudinal (R_{xx}) and transverse (R_{xy}) resistances were obtained by applying a DC current of $I = 1\text{--}10 \mu\text{A}$ to the source and drain leads of the device and by measuring the resulting DC voltage drops V_{xx} and V_{xy} [Fig. 1(a)].

We studied the magnetotransport behavior of ten devices fabricated using thin $(\text{Bi}_2)_5(\text{Bi}_2\text{Se}_3)_7$ films with a thickness of 12 nm from multiple MBE runs under identical growth conditions. Figure 1(b) shows the representative temperature dependent resistivity $\rho_{xx}(T)$ (sample B). ρ_{xx} decreases with decreasing temperature, which can be attributed to a reduction of electron–phonon interaction and which is a characteristic of metallic samples.¹³ At low temperatures ($T < 20$ K), a resistance minimum can be observed [see Fig. 2(a)]. We attribute this to Kondo correlations¹⁴ present in the $(\text{Bi}_2)_5(\text{Bi}_2\text{Se}_3)_7$ films [see Fig. 2(a) and discussion below]. The metallic behavior of the samples is further reflected by the high carrier density of $6 \pm 3 \times 10^{21} \text{ cm}^{-3}$ [carrier mobility $5 \pm 3 \text{ cm}^2(\text{V s})^{-1}$] obtained from measurements of $\rho_{xx}(B)$ and $\rho_{xy}(B)$ [see Figs. 1(c) and 1(d) for such data on sample B]. The observed metallic behavior is in agreement with recent angle-resolved photo electron microscopy experiments, which found that natural heterostructures of Bi-bilayers and Bi_2Se_3 quintuple layers are bulk semi-metals that possess metallic, topological surface states.^{6,15} The magnetoresistance is quadratic at high fields and shows a cusp due to weak-antilocalization at low fields (see discussion in the supplementary material).

We further note a non-linearity in $\rho_{xy}(B)$ measurements [Fig. 1(d)]. This could indicate transport via different electronic bands or spatially separated parallel conducting channels with different carrier mobilities and concentrations.^{16–18}

Alternatively, as we will discuss below, this non-linearity in the Hall effect can indicate an anomalous Hall contribution to $\rho_{xy}(B)$ induced by the presence of magnetic scatters inside our sample, similar to previous findings in magnetically doped Bi_2Se_3 .¹⁹

In the following, we investigate the non-monotonic temperature dependence of the electrical resistance of $(\text{Bi}_2)_5(\text{Bi}_2\text{Se}_3)_7$ films, which we attribute to the Kondo effect induced by local magnetic

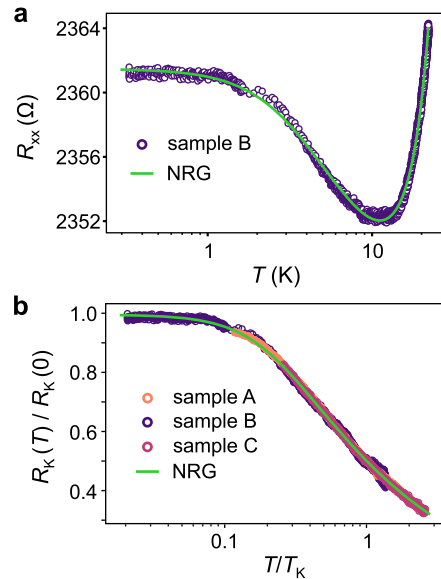


FIG. 2. (a) Temperature-dependent longitudinal resistance of sample B (purple open circles) and a fit using Eq. (1) (green line). A field of $B = 1$ T was applied. (b) Normalized Kondo resistivity as a function of temperature (normalized by the Kondo temperature) for samples A–C (open circles) together with the universal functional predicted by NRG calculations (green line).

scatters. Figure 2(a) shows the four-terminal resistance of sample B as a function of temperature measured at $B = 1$ T. This magnetic field was applied to suppress contributions from localization effects (WAL/WL)²⁰ and is well below the critical field B_c necessary to overcome the Kondo gap for a $S = 1/2$ system at $T \ll T_K = 15$ K (see discussion below), where $B_c = 0.5k_B T_K / (g\mu_B) \approx 6$ T.²¹ We observe a logarithmic increase of R_{xx} below a temperature of 10 K followed by a saturation below 1 K. Such saturation disagrees with (anti-)localization effects where $\partial R / \partial T \propto -\ln T$ for $T \rightarrow 0$ and indicates the absence of a disorder-induced metal to insulator transition or the opening of a bandgap.²⁰

In metallic systems containing magnetic impurities, the conduction electrons can couple anti-ferromagnetically to the local magnetic moments of the impurities. This enables a new spin-flip scattering process with an anomalous component of the resistance $R_K(T/T_K)$, which is approximately logarithmic in T when $T \approx T_K$. Below this characteristic Kondo temperature T_K , thermal fluctuations become weaker than the exchange energy and a so-called Kondo cloud is formed in which conduction electrons screen the local magnetic impurities. This leads to a saturation of the resistance. To this end, the temperature dependent resistance of the sample can be modeled as

$$R(T) = R_0 + qT^2 + pT^5 + R_K\left(\frac{T}{T_K}\right), \quad (1)$$

where R_0 is the residual resistance due to sample disorder and the terms proportional to T^2 and T^5 describe contributions by electron–electron and electron–phonon interactions.²² The contribution of the Kondo effect is described by the following empirical formula:

$$R_K\left(\frac{T}{T_K}\right) = R_K(0) \left(\frac{T_K^2}{T^2 + T_K^2} \right)^s, \quad (2)$$

where $T'_K = T_K/(2^{1/s} - 1)^{1/2}$. Assuming magnetic impurities with spin $S = 1/2$, the numerical factor becomes $s = 0.2225$.

A fit to our experimental data using Eq. (1) is shown in Fig. 2(a) and yields $R_0 = 2330 \Omega$, $q = 2.4 \times 10^{-2} \Omega/K^2$, $p = 1.6 \times 10^{-6} \Omega/K^5$, $R_K(0) = 30.8 \Omega$, and $T_K = 16 \text{ K}$. These parameters can be used to re-scale the experimental data of various samples and compare their normalized Kondo resistivity $R_K(T)/R_K(0)$ vs T/T_K to the universal Kondo behavior from numerical renormalization group calculations (NRG).²³ Such scaling is shown Fig. 2(b). We observe that all experimental curves follow an universal functional and that this functional can be well described by the NRG calculations for the Kondo effect.

In order to find the origin of magnetic scatterers in our sample, we performed first-principles simulations, based on density functional theory (DFT), of $\text{Bi}_2/(\text{Bi}_2\text{Se}_3)_n$ stacks, including different intrinsic point defects. The atomic configuration and energy band structure of $\text{Bi}_2/\text{Bi}_2\text{Se}_3$ are shown in Figs. 3(a) and 3(b), respectively. The system is predicted to be semi-metallic, in agreement with other DFT calculations reported in the literature.^{6,15} Various intrinsic point defects in 2D $\text{Bi}_2/\text{Bi}_2\text{Se}_3$ stacks were first investigated using (3×3) supercells. We considered Bi (V_{Bi}) and Se (V_{Se}) vacancies and Bi (Bi_{Se}) and Se (Se_{Bi}) antisites, present at different locations in the $\text{Bi}_2/\text{Bi}_2\text{Se}_3$ stack, as shown in Fig. S1 (see the supplementary material). All these defects have relatively low formation energies, lying typically between 0.5 and 2 eV (see Fig. S2), except for Se_{Bi} , which has a negative formation energy, with this defect being spontaneously formed in the 2D material. Surprisingly, none of these defects have a net magnetic moment; this can be attributed to the charge transfer occurring between the Bi_2 and Bi_2Se_3 layers. Indeed, the Bi_2 layer tends to give electrons (about $7.8 \times 10^{13} e/\text{cm}^2$) to the Bi_2Se_3 layer,²⁴ which leads to an empty (defect in Bi_2) or fully occupied (defect in Bi_2Se_3) defect level, the defect then being non-magnetic. As shown in the supplementary material (see Fig. S3), when the distance between the Bi_2 and Bi_2Se_3 layers is artificially increased, which results in a reduced charge transfer between these layers, the magnetic moment of some defects “reappears.” We next considered defects in a $\text{Bi}_2/(\text{Bi}_2\text{Se}_3)_2$ stack. The calculated charge

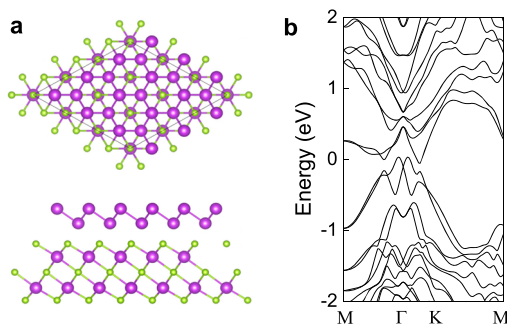


FIG. 3. (a) Top and side views of the atomic structure of $\text{Bi}_2/\text{Bi}_2\text{Se}_3$. The green and purple spheres correspond to the Se and Bi atoms, respectively. (b) Energy band structure of $\text{Bi}_2/\text{Bi}_2\text{Se}_3$. The reference (zero) energy level corresponds to the Fermi level.

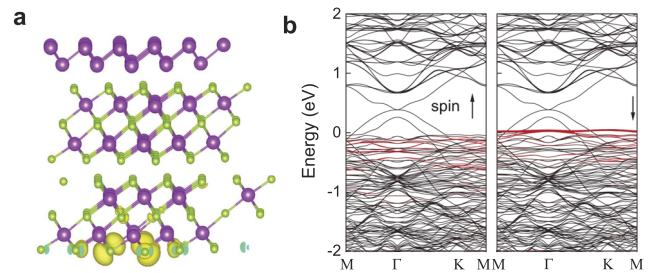


FIG. 4. (a) Atomic structure of a $\text{Bi}_2/(\text{Bi}_2\text{Se}_3)_2$ stack with a Bi vacancy in the bottom Bi_2Se_3 layer. The band-decomposed charge densities in the energy range between -0.02 and 0.03 eV are also shown in yellow. (b) Projected band structures of the system for spin-up and spin-down electrons. The red lines correspond to the contributions from the $4p$ -Se orbitals around the Bi vacancy.

transfer to the bottom Bi_2Se_3 layer is reduced by about an order of magnitude, as compared to the top Bi_2Se_3 layer. We studied the same defects as discussed above, present at different possible sites in the bottom Bi_2Se_3 layer, and identified only one defect with a net magnetic moment of about $0.55 \mu_B$, namely, a Bi vacancy. The atomic configuration of the corresponding defective structure is shown in Fig. 4(a). The formation energy of this Bi vacancy in the $\text{Bi}_2/(\text{Bi}_2\text{Se}_3)_2$ structure lies between about 0.5 and 1 eV, in the Se-rich and Bi-rich limit, respectively. As shown in Fig. 4(b), localized states, corresponding to the $4p$ -Se orbitals neighboring the Bi vacancy site, are clearly observed in the electronic density of states within an energy range between 0 and 0.5 eV from the Fermi level E_F . The spin-polarized energy band structure also indicates the presence of localized spin-down states near E_F , associated with the $4p$ -Se orbitals. We thus tentatively assign the magnetic defects responsible for the Kondo effect observed in our samples to these Bi vacancies.

SUMMARY

To summarize, we present a hybrid epitaxy approach, PA-MBE, suitable to grow high-quality thin films of the topological semimetal $(\text{Bi}_2)_5(\text{Bi}_2\text{Se}_3)_7$. Depth cryogenic magnetotransport experiments combined with first-principle simulations allowed us to reveal that Bi vacancies could act as intrinsic magnetic scatterers in this material. These scatterers explain the observed pronounced Kondo effect in the temperature dependent longitudinal resistance of the devices. Therefore, our work highlights how intrinsic impurities can strongly impact topological properties, an important finding when considering topological materials for future device integration.

SUPPLEMENTARY MATERIAL

The supplementary material contains experimental details about crystal growth and characterization (Raman, TEM, RHEED, XRD, RBS), atomic force microscopy, details about weak-antilocalization and computational methods.

ACKNOWLEDGMENTS

The authors thank T. Costi for helpful discussions about the Kondo data and A. Dixit for supporting the evaluation of the WAL

data. The authors acknowledge the Horizon 2020 project SKYTOP Skyrmion-Topological insulator and Weyl semimetal technology (FETPROACT-2018-01, No. 824123). P.G. acknowledges financial support from the F.R.S.-FNRS of Belgium (Grant Nos. FNRS-CQ-1.C044.21-SMARD, FNRS-CDR-J.0068.21-SMARD, and FNRS-MIS-F.4523.22-TopoBrain), from the Federation Wallonie-Bruxelles through the ARC under Grant Nos. 21/26-116, and from the EU (Grant No. ERC-StG-10104144-MOUNTAIN). This project (Grant No. 40007563-CONNECT) received funding from the FWO and F.R.S.-FNRS under the Excellence of Science (EOS) program. V.F. acknowledges financial support from the F.R.S.-FNRS of Belgium (Grant No. FNRS-FRIA-1.E092.23-TOTEM). C.M. acknowledges an ERC-CoG No. 864483 NOTICE. Part of this work was financially supported by the KU Leuven Research Fund, Project No. C14/21/083. Part of the computational resources and services used in this work was provided by the VSC (Flemish Supercomputer Center), funded by the Research Foundation Flanders (FWO) and the Flemish Government – department EWI.

AUTHOR DECLARATIONS

Conflict of Interest

The authors have no conflicts to disclose.

Author Contributions

Pascal Gehring: Conceptualization (lead); Data curation (lead); Formal analysis (lead); Investigation (lead); Methodology (lead); Writing – original draft (lead). **Clement Merckling:** Formal analysis (equal); Investigation (equal); Methodology (equal); Writing – review & editing (equal). **Ruishen Meng:** Formal analysis (equal); Methodology (equal); Writing – review & editing (equal). **Valentin Fonck:** Formal analysis (equal); Validation (equal); Writing – review & editing (equal). **Bart Raes:** Methodology (equal); Writing – review & editing (equal). **Michel Houssa:** Supervision (equal); Writing – review & editing (equal). **Joris Van de Vondel:** Supervision (equal); Writing – review & editing (equal). **Stefan De Gendt:** Supervision (equal); Writing – review & editing (equal).

DATA AVAILABILITY

The data that support the findings of this study are available from the corresponding author upon reasonable request.

REFERENCES

- W. Han, Y. Otani, and S. Maekawa, “Quantum materials for spin and charge conversion,” *Npj Quantum Mater.* **3**, 27 (2018).
- Devender, P. Gehring, A. Gaul, A. Hoyer, K. Vaklinova, R. J. Mehta, M. Burghard, T. Borca-Tasciuc, D. J. Singh, K. Kern, and G. Ramanath, “Harnessing topological band effects in bismuth telluride selenide for large enhancements in thermoelectric properties through isovalent doping,” *Adv. Mater.* **28**, 6436 (2016).
- H. Yang, W. You, J. Wang, J. Huang, C. Xi, X. Xu, C. Cao, M. Tian, Z.-A. Xu, J. Dai, and Y. Li, “Giant anomalous N effect in the magnetic W semimetal $\text{Co}_3\text{Sn}_2\text{S}_2$,” *Phys. Rev. Mater.* **4**, 024202 (2020).
- Y. Okazaki, T. Oe, M. Kawamura, R. Yoshimi, S. Nakamura, S. Takada, M. Mogi, K. S. Takahashi, A. Tsukazaki, M. Kawasaki, Y. Tokura, and N.-H. Kaneko, “Quantum anomalous hall effect with a permanent magnet defines a quantum resistance standard,” *Nat. Phys.* **18**, 25 (2021).
- A. Toniato, B. Gotsmann, E. Lind, and C. B. Zota, “Weyl semi-metal-based high-frequency amplifiers,” in *2019 IEEE International Electron Devices Meeting (IEDM)* (IEEE, 2019), pp. 9.4.1–9.4.4.
- Q. D. Gibson, L. M. Schoop, A. P. Weber, H. Ji, S. Nadj-Perge, I. K. Drozdov, H. Beidenkopf, J. T. Sadowski, A. Fedorov, A. Yazdani, T. Valla, and R. J. Cava, “Termination-dependent topological surface states of the natural superlattice phase Bi_4Se_3 ,” *Phys. Rev. B* **88**, 081108 (2013); [arXiv:1305.3558](https://arxiv.org/abs/1305.3558).
- A. P. Weber, Q. D. Gibson, H. Ji, A. N. Caruso, A. V. Fedorov, R. J. Cava, and T. Valla, “Gapped surface states in a strong-topological-insulator material,” *Phys. Rev. Lett.* **114**, 256401 (2015).
- Z. F. Wang, M.-Y. Yao, W. Ming, L. Miao, F. Zhu, C. Liu, C. L. Gao, D. Qian, J.-F. Jia, and F. Liu, “Creation of helical Dirac fermions by interfacing two gapped systems of ordinary fermions,” *Nat. Commun.* **4**, 1384 (2013).
- M. Samanta and K. Biswas, “2D nanosheets of topological quantum materials from homologous $(\text{Bi}_2)_m(\text{Bi}_2\text{Se}_3)_n$ heterostructures: Synthesis and ultralow thermal conductivity,” *Chem. Mater.* **32**, 8819 (2020).
- S. El Kazzi, W. Mortelmans, T. Nuytten, J. Meersschaut, P. Carolan, L. Landeloos, T. Conard, I. Radu, M. Heyns, and C. Merckling, “ MoS_2 synthesis by gas source MBE for transition metal dichalcogenides integration on large scale substrates,” *J. Appl. Phys.* **123**, 135702 (2018).
- W. Mortelmans, A. Nalin Mehta, Y. Balaji, S. El Kazzi, S. Sergeant, M. Houssa, S. De Gendt, M. Heyns, and C. Merckling, “Fundamental limitation of van der Waals homoepitaxy by stacking fault formation in WSe_2 ,” *2D Mater.* **7**, 025027 (2020).
- P. Gehring, F. B. Reusch, S. S. Mashhadi, M. Burghard, and K. Kern, “Surface oxidation effect on the electrical behaviour of $\text{Bi}_2\text{Te}_2\text{Se}$ nanoplatelets,” *Nanotechnology* **27**, 285201 (2016).
- P. Gehring, B. Gao, M. Burghard, and K. Kern, “Two-dimensional magnetotransport in $\text{Bi}_2\text{Te}_2\text{Se}$ nanoplatelets,” *Appl. Phys. Lett.* **101**, 023116 (2012).
- J. Kondo, “Resistance minimum in dilute magnetic alloys,” *Prog. Theor. Phys.* **32**, 37 (1964), <https://academic.oup.com/ptp/article-pdf/32/1/37/5193092/32-1-37.pdf>.
- T. Valla, H. Ji, L. M. Schoop, A. P. Weber, Z. H. Pan, J. T. Sadowski, E. Vescovo, A. V. Fedorov, A. N. Caruso, Q. D. Gibson, L. Muehler, C. Felser, and R. J. Cava, “Topological semimetal in a $\text{Bi}-\text{Bi}_2\text{Se}_3$ infinitely adaptive superlattice phase,” *Phys. Rev. B* **86**, 241101 (2012); [arXiv:1208.2741](https://arxiv.org/abs/1208.2741).
- J. S. Kim, S. S. A. Seo, M. F. Chisholm, R. K. Kremer, H.-U. Habermeier, B. Keimer, and H. N. Lee, “Nonlinear hall effect and multichannel conduction in $\text{LaTiO}_3/\text{STO}_3$ superlattices,” *Phys. Rev. B* **82**, 201407 (2010).
- Z. Ren, A. A. Taskin, S. Sasaki, K. Segawa, and Y. Ando, “Large bulk resistivity and surface quantum oscillations in the topological insulator $\text{Bi}_2\text{Te}_2\text{Se}$,” *Phys. Rev. B* **82**, 241306 (2010).
- P. Gehring, B. F. Gao, M. Burghard, and K. Kern, “Growth of high-mobility $\text{Bi}_2\text{Te}_2\text{Se}$ nanoplatelets on hBN sheets by van der Waals epitaxy,” *Nano Lett.* **12**, 5137 (2012).
- M. Liu, J. Zhang, C.-Z. Chang, Z. Zhang, X. Feng, K. Li, K. He, L.-L. Wang, X. Chen, X. Dai, Z. Fang, Q.-K. Xue, X. Ma, and Y. Wang, “Crossover between weak antilocalization and weak localization in a magnetically doped topological insulator,” *Phys. Rev. Lett.* **108**, 036805 (2012).
- J.-H. Chen, L. Li, W. G. Cullen, E. D. Williams, and M. S. Fuhrer, “Tunable Kondo effect in graphene with defects,” *Nat. Phys.* **7**, 535 (2011).
- Y.-h. Zhang, S. Kahle, T. Herden, C. Strohm, M. Mayor, U. Schlickum, M. Ternes, P. Wahl, and K. Kern, “Temperature and magnetic field dependence of a Kondo system in the weak coupling regime,” *Nat. Commun.* **4**, 2110 (2013).
- M. Lee, J. R. Williams, S. Zhang, C. D. Frisbie, and D. Goldhaber-Gordon, “Electrolyte gate-controlled Kondo effect in ST_3 ,” *Phys. Rev. Lett.* **107**, 256601 (2011).
- T. A. Costi, A. C. Hewson, and V. Zlatic, “Transport coefficients of the Anderson model via the numerical renormalization group,” *J. Phys.: Condens. Matter* **6**, 2519 (1994).
- K. Govaerts, K. Park, C. De Beule, B. Partoens, and D. Lamoen, “Effect of Bi bilayers on the topological states of Bi_2Se_3 : A first-principles study,” *Phys. Rev. B* **90**, 155124 (2014).